

# Structure Thermal Domain Size in $\mu\text{m}$ -Thick Single Crystalline Sapphire Wafer Uncovered by Low-Momentum Phonon Scattering

John Bai, Amin Karamati, Xinyue Duan, Huan Lin,\* and Xinwei Wang\*



Cite This: *J. Phys. Chem. C* 2025, 129, 5754–5761



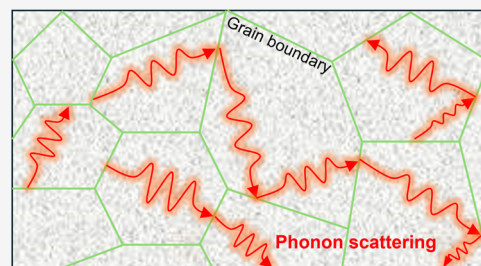
Read Online

ACCESS |

Metrics & More

Article Recommendations

**ABSTRACT:** The structure thermal domain (STD) size is a characteristic size that reflects the defect-energy carrier scattering. To date, it is still unclear how a material's grain structural characteristics are related to and determine the STD size. This work presents the first effort on such physics by measuring the STD size of  $\mu\text{m}$ -thick single crystalline sapphire wafers and interpreting it based on the crystallite size uncovered by X-ray diffraction (XRD). A novel measurement methodology is developed to measure the thermal reffusivity ( $\Theta$ ) at the zero temperature rise limit. This allows for high-precision determination of  $\Theta$  at the 0 K limit ( $\Theta_0$ ).  $\Theta_0$  eliminates the effect of Umklapp phonon scattering and is solely determined by the grain boundary scattering of low-momentum phonons. Based on  $\Theta_0$ , the STD size is found to be 85.1 nm in the wafer's in-plane direction, while the XRD uncovers crystallite sizes of 283 nm in the cross-plane direction and 34.4 nm in the in-plane direction. The STD size is influenced by phonon scattering in all directions, more so by that in the heat conduction direction. It provides a new aspect in understanding the grain characteristic size from the viewpoint of phonon transport with a direction dependence.



## 1. INTRODUCTION

The thermal reffusivity ( $\Theta$ ) concept was developed to directly correlate energy carrier scattering and material's structural defects.<sup>1</sup> The widely used thermal conductivity ( $k$ )–temperature ( $T$ ) correlation carries a very strong effect of the temperature dependence of specific heat, making it hard to uncover the effect of defect-energy carrier scattering.  $\Theta$  is the energy carriers' volumetric specific heat divided by their  $k$ . It groups the energy carrier scattering under the single relaxation time frame and always decreases with decreased temperature as long as the material's structure is physically stable upon temperature change. For isotropic nonmetallic materials whose  $k$  is sustained by phonon transport,  $\Theta$  is the inverse of its thermal diffusivity ( $\alpha$ ):  $\Theta = 1/\alpha$ . At the 0 K limit, the phonon population involved in Umklapp scattering decreases to a minimal level and has very low momentum (small wave vector). Hence, defect scattering within the sample dominates and controls  $\Theta$ .<sup>2–6</sup> The  $\Theta$  value at the 0 K limit denoted as  $\Theta_0$  (termed “residual thermal reffusivity”) is solely determined by the defect scattering of low-momentum phonons and can be used to determine the structural thermal domain (STD) size, a size reflected by the low-momentum phonon mean free path (MFP) at the 0 K limit.

Our previous work investigated different aspects of  $\Theta$ . Furthermore, experiments on microscale ultrahigh-molecular-weight polyethylene (UHMWPE) fibers also explored  $\Theta$  and how defects can affect the STD size.<sup>7</sup> In 2018, another breakthrough was made where  $\Theta$  was used to evaluate amorphous material's STD size in comparison with structure

characterization by X-ray diffractometry (XRD).<sup>8</sup> The  $\Theta$  was used once again in our lab to investigate the STD size of  $\text{MoSe}_2$  and compare it with the crystallite size of bulk  $\text{MoSe}_2$ .<sup>9</sup> Very recently,  $\Theta$  was used to report the axis-direction STD size of single-walled carbon nanotube (SWCNT) bundles of <10 nm diameter.<sup>10</sup> Also, after introducing a concept of anisotropic specific heat, the thermal reffusivity theory has been used to report the first sub $\mu\text{m}$  scale STD size in the  $c$ -axis direction of graphene paper.<sup>11</sup>

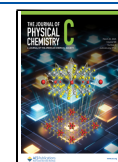
It is noted that for crystallite size characterization, XRD has been used widely, and the crystallite size is very well-defined, and its physics is very well understood. However, if a material has an extremely small scattering cross section (e.g., cross-plane of two-dimensional (2D) materials, nanowires, and nanotubes), then XRD could not have enough scattering to generate the needed diffraction patterns. Also, for amorphous materials, XRD could not generate a meaningful peak for structural size determination. In extremely high-quality crystals, the crystallite size will make the XRD peak too narrow to measure (even narrower than the machine limit). Under these scenarios, the thermal reffusivity concept provides a very

**Received:** January 7, 2025

**Revised:** February 26, 2025

**Accepted:** February 28, 2025

**Published:** March 7, 2025



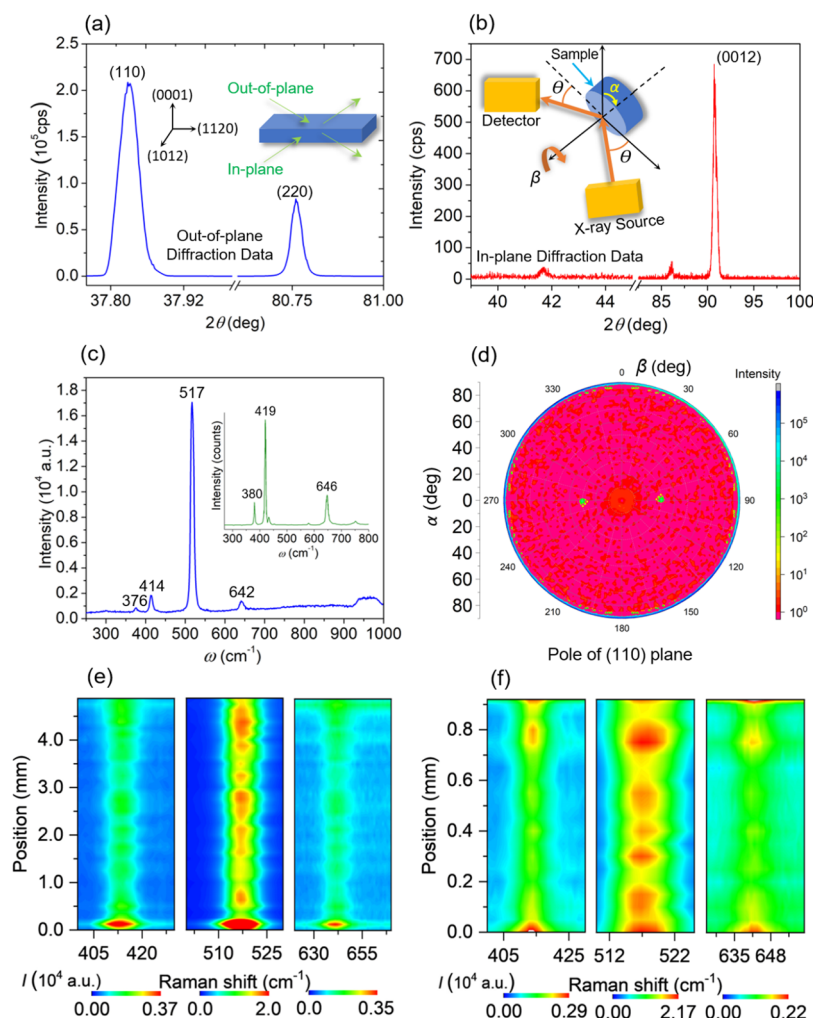


**Figure 1.** (a) Out-of-plane and (b) in-plane XRD peaks. Both show the Miller indices and direction of the XRD scan. (b) Diagram of the in-plane pole-figure XRD analysis of the sapphire sample. (c) Out-of-plane Raman spectrum. The inset shows the Raman spectrum of sapphire from the literature<sup>13</sup> for comparison purposes. (d) XRD pole-figure plot for the (110) plane. In-plane Raman spectrum scanning along the (e) (1120) direction (length) and (f) (1012) direction (width) was used to study the structure uniformity.

compelling method to characterize the structural domain size based on energy carrier scattering.

It should be noted that the XRD crystallite size and STD size would not necessarily be the same although they could be very close.<sup>10</sup> All of our past work on STD size determination and comparison with the crystallite size determined by XRD was done for polycrystalline or amorphous materials. Strict determination of the STD size and comparison with XRD crystallite size for single crystals is of great importance in evaluating their relation and understanding the physics behind the STD size. In this paper, the STD size of a  $\mu\text{m}$ -thick sapphire single crystal wafer is studied for the first time, which eliminates other factors on STD size and provides in-depth insight into its physics. Here, we measure the  $\alpha$  of a  $\mu\text{m}$ -thick single crystalline sapphire wafer of  $1\text{ mm} \times 5\text{ mm} \times 25\ \mu\text{m}$  size from room temperature (RT) down to 13 K. Several properties are studied, including  $\alpha$ ,  $k$ ,  $\Theta$ , and the STD size determined based on  $\Theta_0$ . A comparison is made between the STD size and the XRD crystallite size. In-depth discussions of the thermal diffusivity theory, the physics of STD size, and the mechanisms behind it are provided.

## 2. SAMPLE STRUCTURE

The sapphire (alpha alumina) wafer sample used in the experiment is obtained from Valley Design Corporation. The company employs DDISCO and K&S saws to dice wafers to microlevel tolerance. For this specific sapphire wafer (A-plane wafer), the size is 5 mm in length, 1 mm in width, and  $25\ \mu\text{m}$  in thickness. The sample is then optically polished on both sides with a 60/40 scratch/dig. In this work, the structure of the sample is characterized using Raman spectroscopy and XRD. Figure 1 shows the Raman spectrum and XRD characterization of our sample. The tests conducted are in-plane and out-of-plane XRD analyses to determine the crystallite size. Figure 1a,b shows the XRD peaks obtained from that analysis. The crystallite sizes are determined for different plane directions using the full width at half-maximum (FWHM). The out-of-plane XRD gives the (110) crystallite size as 283 nm. The in-plane direction XRD gives the (0012) crystallite size as 34.4 nm. The in-plane size is further confirmed by the literature that  $\alpha$  alumina's crystalline size is normally around 33 nm.<sup>12</sup> While the out-of-plane peaks are quite sharp and easy to measure, there is some disturbance with the in-plane peaks. Therefore, the in-plane crystallite size measurement is less accurate than the out-of-plane one. The

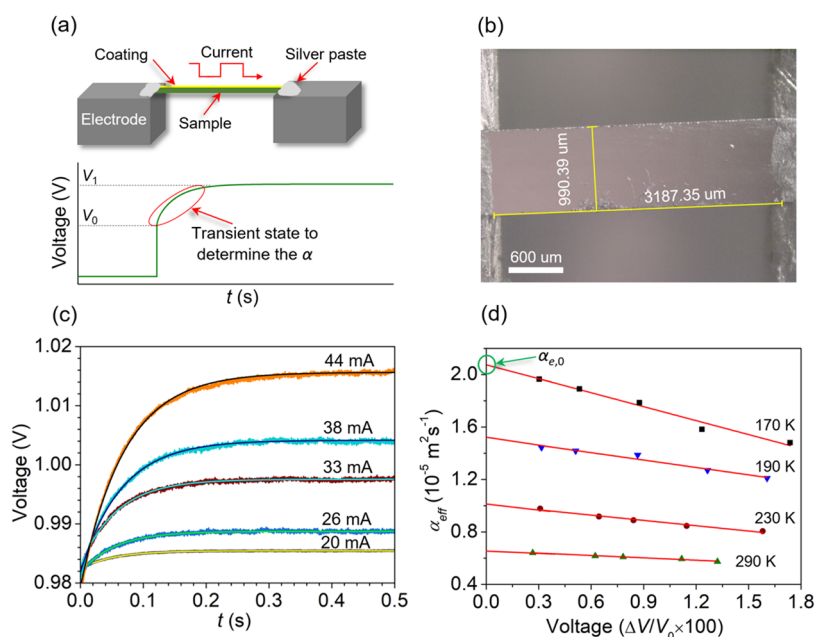


**Figure 2.** (a) Schematic of the TET technique. A schematic of voltage evolution is also shown at the bottom of the figure. (b) Microscopic view of the sapphire wafer sample connected between two electrodes with the length and width dimensions. (c) Experimental results for the voltage change versus time using different currents at 170 K. This is done over all other temperatures to obtain  $\alpha$  at the zero temperature rise limit. (d)  $\alpha_{\text{eff}}$  vs voltage % change, which is used to find the  $\alpha_{\text{eff}}$  at zero temperature rise limit ( $\alpha_{e,0}$ ). This is critical to obtaining a more accurate picture of  $\alpha_{\text{eff}}$  at specific temperatures.

very large out-of-plane crystallite size also validates the single crystal claim from the vendor.

Pole-figure XRD is also conducted for our sample to characterize its crystalline orientation. A physical representation of the test is shown in the inset of Figure 1b. The two axes ( $2\theta$ ) are used to set the X-ray source and detector configuration and determine the Miller indices of the pole figure. The third and fourth axes,  $\alpha$  and  $\beta$ , are used to tilt and spin the specimen, respectively, in regard to the X-ray source and detector in order to determine features like crystalline orientation. Figure 1d shows the pole plot of the (110) plane. It is evident that this plane is highly aligned along the out-of-plane direction. Raman spectroscopy is also conducted on the sample to compare with the literature results to check possible structure variations or irregularities.<sup>2,14</sup> Since sapphire is such a common material, there is plenty of Raman spectrum literature to compare with. Two Raman scans (laser irradiation along the out-of-plane direction) are conducted in the length and width directions of the sample. Both scans are done with the sapphire sample supported on a silicon wafer. Figure 1c compares the Raman spectrum of our sample with that of the literature (the inset in Figure 1c).<sup>13</sup> It is obvious that the Raman peaks of our sample at 376, 414, and 641  $\text{cm}^{-1}$  almost match the peaks from the literature at 380, 419, and 646  $\text{cm}^{-1}$ . The slight difference is more likely due to a system-induced shift. The Raman peak at 517  $\text{cm}^{-1}$  is for the silicon substrate.<sup>15</sup> In Figure 1e,f, the middle column representing the silicon peak is much stronger than the sapphire peaks but is not uniform in intensity, with a slight variation throughout the scanning. This could be due to optical interference throughout the scans due to sapphire sample thickness nonuniformity and varied sample-substrate spacing.<sup>9</sup> The sapphire Raman intensity overall is weak, except for the edge region. The high Raman intensity at the edges could be due to more local defects in sapphires due to dicing. The defects at the edges will have increased grain boundary

densities, which cause multiple laser reflections within the sample and, thus, increase the Raman scattering intensity. Such an edge effect has been observed in our lab for silicon wafers.<sup>16</sup> Comparing Figure 1e and f shows this edge effect is more prominent in the width direction (Figure 1f). This is attributed to the wafer dicing and polishing processes. Our optical microscopic study reveals that the edges at the end of the width direction are rougher and have more surface cracks than those at the end of the length direction. This leads to a higher density of grain boundaries inside, which will induce more laser reflection and a stronger Raman signal.

### 3. THERMAL DIFFUSIVITY MEASUREMENT AT THE LIMIT OF ZERO TEMPERATURE RISE

In this work, the transient electrothermal (TET) technique is used to measure the sapphire wafer's  $\alpha$  in the in-plane direction. The TET technique is a quick and reliable method for measuring a suspended film/fiber's  $\alpha$ , whether it is electrically conductive or not. It has proved to be a potent method since its introduction in 2007 by our lab.<sup>17</sup> The main advantage of the TET is that it can measure the  $\alpha$  at the micro/nanoscale for fiber or film-like materials with much-improved control and accuracy over other frequency-domain techniques.<sup>18–21</sup> Here, we conduct further development of the TET technique to measure  $\alpha$  at the limit of zero temperature rise. Such capability is critical for measurement at cryogenic temperatures, for uncovering the variation of thermal diffusivity with temperature, and for determining the residual thermal diffusivity at the 0 K limit.

The schematic of the TET technique is shown in Figure 2a. The sample is connected to two aluminum electrodes by using silver paste to ensure sound electrical and thermal contacts. Since the sapphire wafer is not electrically conductive, a 15 nm Ir film is coated on its surface to make it electrically conductive. The effect of this Ir coating will be discussed

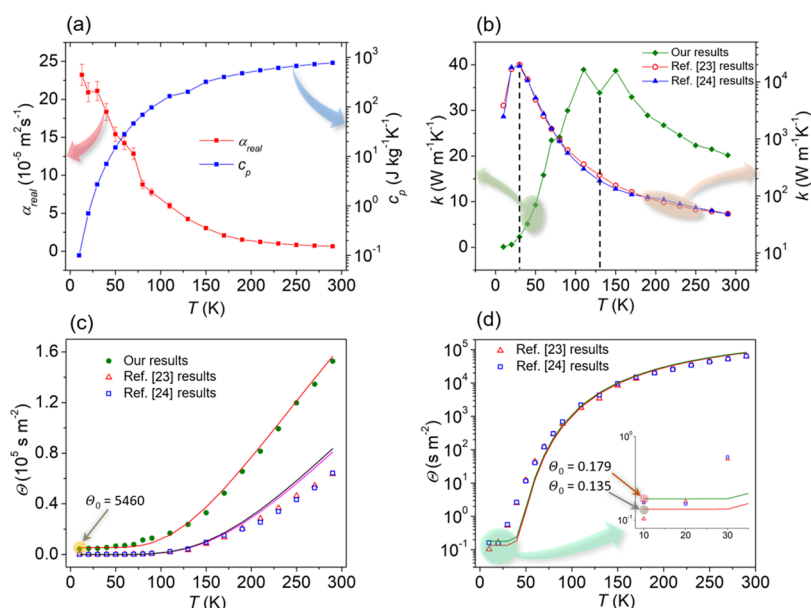


**Figure 3.** (a) Intrinsic (real)  $\alpha$  at different temperatures ( $\alpha_{\text{real}}$ ) for our sapphire sample and the  $c_p$  variation with temperature from the literature.<sup>23</sup> (b) Our determined  $k$  in comparison with literature data.<sup>23,24</sup> (c)  $\Theta$  variation with temperature for our sample and those from the literature. The solid lines are for the fitting based on eq 5 using the relative standard deviation method.<sup>23,24</sup> (d)  $\Theta$  fitting of literature data in logarithmic scale to detail the low-temperature region, as highlighted in the inset.

later. Figure 2b shows the sapphire wafer sample measured in our work. A step DC current (Keithley 6221) is fed through the sample to introduce Joule heating. The Joule heating will lead to a temperature rise that will also cause the sample's resistance to change. As a result, the voltage over the sample will change accordingly. An oscilloscope (Tektronix DPO3052) is used to track the transient behavior of the voltage change. This transient behavior, as shown in Figure 2a, can be used to determine  $\alpha$ . The voltage change is linearly proportional to the average temperature increase of the sample under moderate heating. After measurement, the voltage change is normalized to represent the normalized temperature change, which is fitted to determine  $\alpha$ . The governing equation for heat conduction along the sample in the length ( $x$ ) direction is<sup>22</sup>

$$\frac{\partial(\rho c_p T)}{\partial t} = k \frac{\partial^2 T}{\partial x^2} + \dot{q} \quad (1)$$

Here,  $\rho$  and  $c_p$  are the density and specific heat of the sample.  $\dot{q}$  is the equivalent volumetric heat source caused by Joule heating. Given the overall situation, the initial condition for the problem is  $T(x, t = 0) = T_0$  ( $T_0$ : ambient temperature). Since the aluminum base can be treated as a heat sink, we have boundary conditions of  $T(x = 0, t) = T(x = L, t) = T_0$ .  $L$  is the sample's length. Subsequently, the normalized temperature rise  $T^*(t) = [T(t) - T_0]/(T_1 - T_0)$  can be solved as<sup>22</sup>

$$T^* = \frac{96}{\pi^4} \sum_{m=1}^{\infty} \frac{1 - \exp[-(2m-1)^2 \pi^2 \alpha_{\text{eff}} t / L^2]}{(2m-1)^4} \quad (2)$$

where  $\alpha_{\text{eff}}$  is the sample's effective thermal diffusivity, which includes the effect of radiation and the iridium coating on the sapphire surface. Here,  $T_1$  is the steady state temperature after applying the step DC current. After the voltage evolution is measured, the experimental normalized temperature increase is calculated as  $T_e^*(t) = [V(t) - V_0]/(V_1 - V_0)$ , where  $V_0$  and  $V_1$

are the initial and final voltages over the sample, shown in Figure 2a schematically.

As shown in Figure 2b, the measured sample is 3.187 mm long and 0.990 mm wide. The sample is placed in a cryogenic station (CCS-450, JANIS) under a vacuum below 1 mTorr. This vacuum is needed to eliminate the thermal convection effect around the sample. In TET measurement, due to the temperature increase upon Joule heating, the measurement of  $\alpha$  will not be at ambient  $T_0$ . In the TET experiment, usually, a voltage change of 0.3% is needed for obtaining a sound  $V-t$  signal to determine  $\alpha$  with a high accuracy. At high temperatures (e.g.,  $>50$  K), a voltage change of 0.3% needs a temperature rise of 1 K or more<sup>7</sup> for the sample. However, when the ambient temperature is low, such as 50 K or lower, the temperature coefficient of electrical resistance becomes very small. So, a 0.3% voltage change corresponds to a much higher temperature rise. Therefore, at low temperatures, the measured  $\alpha$  does not present the one at ambient temperature; rather, it is for a much higher temperature. This makes it very difficult to obtain the real  $\alpha$  at low temperatures.

To obtain the  $\alpha$  at ambient temperature (meaning negligible temperature rise) at each specified ambient temperature point, the TET measurement is conducted using different currents with an upper limit of voltage change of 1.5%. Then, the determined  $\alpha$  is plotted against the relative voltage change ( $\Delta V/V_0 \times 100$ ) to extract the  $\alpha$  at the zero limit of  $\Delta V/V_0$  (meaning zero temperature rise). Figure 2c shows the measurement data at 170 K using different currents. The curves are fitted using eq 2 to determine  $\alpha_{\text{eff}}$  using the least-squares method. Figure 2d shows the determined  $\alpha_{\text{eff}}$  against the relative voltage change for four selected ambient temperature points. Very strikingly, a linear relation is observed between  $\alpha_{\text{eff}}$  and the relative voltage change. So, linear fitting is conducted to determine the  $\alpha_{\text{eff}}$  at zero voltage change ( $\alpha_{e,0}$ ). By doing so,  $\alpha_{\text{eff}}$  can be determined at ambient (initial) temperature. This treatment is critical to our latter study of the  $\Theta$  variation against  $T$ . As shown in Figure 2d, at  $T = 170$  K, for

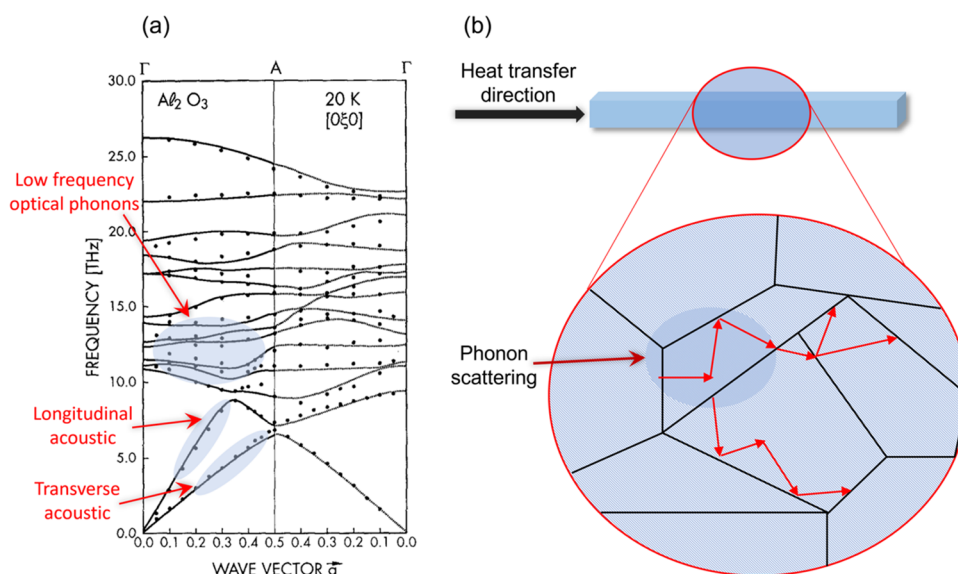


**Figure 4.** (a) Sapphire phonon dispersions acquired from the literature, reproduced with permission from ref 26. Copyright 1969 Springer Nature. Optical and acoustic phonons are labeled for discussion. The transverse acoustic (TA) mode follows the same phonon velocity as the flexural acoustic (ZA) mode. (b) Basic physics demonstration of heat conduction occurring in the in-plane direction of our sample and phonon scattering by grain boundaries.

instance,  $\alpha_{e,0}$  (the intercept of corresponding linear fitting) is obtained as  $2.07 \times 10^{-5} \text{ m}^2 \text{ s}^{-1}$ . Compared with the  $\alpha_{\text{eff}}$  measured using the least current (i.e., 20 mA) for this case ( $1.96 \times 10^{-5} \text{ m}^2 \text{ s}^{-1}$ ),  $\alpha_{e,0}$  shows a 5.6% difference. At low temperatures,  $\alpha_{\text{eff}}$  changes slowly with the temperature slowly. So, a small decrease of  $\alpha_{\text{eff}}$  corresponds to a very large elevation of the sample's temperature over the ambient one. An  $\sim 5\%$  decrease of  $\alpha_{\text{eff}}$  from the real value means the sample's temperature could be around 20–30 K higher than the ambient one. This firmly proves the necessity of this methodology to obtain  $\alpha_{\text{eff}}$  under zero temperature rise, as it improves the measurement temperature accuracy to a much higher level. This is more critical for lower temperature TET measurements and the later data fitting.

#### 4. THERMAL CONDUCTIVITY OF SAPPHIRE WAFER

The obtained  $\alpha_{e,0}$ , in fact, has the effects of radiation and Ir coating. Here, we analyze these effects and prove that they have negligible effects on the intrinsic  $\alpha$  of the sample ( $\alpha_{\text{real}}$ ). By considering these effects,  $\alpha_{\text{real}}$  can be calculated as<sup>7</sup>

$$\alpha_{\text{real}} = \alpha_{e,0} - \frac{8\varepsilon\sigma T^3 L^2}{\pi^2 D \rho c_p} - \frac{L_{\text{Lorenz}} TL}{RA \rho c_p} \quad (3)$$

where  $\varepsilon$  takes 1 to estimate the upper limit of the radiation effect,  $\sigma$  is the Stefan–Boltzmann constant of  $5.67 \times 10^{-8} \text{ Wm}^2 \text{ K}^{-4}$ ,  $D$  is the sample's thickness of 25  $\mu\text{m}$ , and  $L_{\text{Lorenz}}$  is the Lorenz number for iridium, which in this case is  $2.45 \times 10^{-8} \text{ W}\Omega \text{ K}^{-2}$ .<sup>7</sup> The effects of radiation and coating are calculated at two temperatures of 290 and 13 K. At 290 K, the radiation and Ir coating only cause a difference of  $\alpha$  as  $1.48 \times 10^{-7}$  and  $5.69 \times 10^{-9} \text{ m}^2 \text{ s}^{-1}$ , respectively, which are negligible compared with the  $\alpha_{e,0}$  at 290 K ( $6.57 \times 10^{-6} \text{ m}^2 \text{ s}^{-1}$ ). At 13 K, the  $\alpha$  difference caused by radiation and Ir coating is  $1.03 \times 10^{-7}$  and  $2.32 \times 10^{-6} \text{ m}^2 \text{ s}^{-1}$ , respectively, which are still negligible compared with the  $\alpha_{e,0}$  at 13 K ( $2.32 \times 10^{-4} \text{ m}^2 \text{ s}^{-1}$ ).

Figure 3a shows the variation of  $\alpha_{\text{real}}$  with the temperature. It is observed it increases significantly with decreased temperature,

from  $6.57 \times 10^{-6} \text{ m}^2 \text{ s}^{-1}$  at 290 K to  $2.32 \times 10^{-4} \text{ m}^2 \text{ s}^{-1}$  at 13 K. The uncertainty shown in Figure 3a originates from two sources. One is the fitting uncertainty of  $\Delta\alpha$ . For every set of measurements of  $\alpha$  at each ambient temperature, there is an uncertainty with the  $\alpha_{\text{eff}} \sim \Delta V/V_0$  fitting. The other uncertainty is related to the length measurement of the sapphire wafer, as shown in Figure 2b. The  $\alpha$  evaluation is related with  $L^2$ . With both considered, there is less than  $\pm 5\%$  uncertainty for  $\alpha_{\text{real}}$ . The  $k$  value of our sapphire wafer can be calculated as  $k = \alpha_{\text{real}} \rho c_p$ . Figure 3a shows the  $c_p$  of sapphire from RT down to 10 K.<sup>23,24</sup> The density is measured as 3.98  $\text{g cm}^{-3}$ , which is consistent with the literature value of 3.99  $\text{g cm}^{-3}$ .<sup>24</sup> The determined  $k$  is shown in Figure 3b, in comparison with literature data of a very high-purity sapphire. Two observations are made about this comparison. The first one is that the  $k$  of the  $\mu\text{m}$ -thick wafer is much lower than that of high-purity sapphires reported in the literature, especially at cryogenic temperatures. The other observation is that our measured  $k$  has a peak around 130 K, while the literature  $k$  peaks are at a much lower  $T$ , around 30 K. These differences are caused by the high defect level in the  $\mu\text{m}$ -thick sapphire wafer studied in this work.

To explain the underlying physics, the relationship between  $k$  and phonon mean free path (MFP:  $l$ ) under the single relaxation time frame is used

$$k = Cv l/3 \quad (4)$$

where  $v$  is the average phonon velocity and  $C$  is the volumetric specific heat of phonons. Figure 4a shows the sapphire's phonon dispersion curves with the optical and acoustic phonons labeled. For sapphires, several low-frequency branches of optical phonons (shown in Figure 4a) can be readily excited and contribute to  $C$  substantially. However, these optical phonons have very low velocities. This makes the MFP very long. At RT, the MFP of high-purity sapphire was calculated to be around  $120 \pm 10 \text{ nm}$ .<sup>25</sup> For our sapphire wafer, the measured  $k$  is along the in-plane direction. The crystallite size in this direction is only 34.4 nm. This is much

shorter than that of the MFP of high-purity sapphire. Therefore, a significant  $k$  reduction is expected. A more detailed explanation of this physics will be provided based on  $\Theta$  and STD size in the section below.

For the difference in the peak location of  $k$ , it can be explained by the defect effect on MFP. The MFP ( $l$ ) has two contributions as  $l^{-1} = l_U^{-1} + l_d^{-1}$ , where  $l_U$  is caused by phonon-phonon scattering (Umklapp scattering) and  $l_d$  is caused by defect scattering. While  $l_d$  changes little with  $T$ ,  $l_U$  goes up quickly with reduced temperatures because the phonon population involved in Umklapp scattering goes down quickly with temperature reduction. For the measured  $\mu\text{m}$ -thick sapphire wafer in this work, its  $l_d$  is much smaller than that of high-purity sapphire, so at a relatively higher  $T$ , we will have  $l_d^{-1} \gg l_U^{-1}$ , and then the  $k$ - $T$  curve is dominated by the  $C$ - $T$  relation with further  $T$  reduction. This makes the maximum  $k$  appear at a higher  $T$  compared with that of high-purity sapphire.

## 5. THERMAL REFFUSIVITY AND STRUCTURE THERMAL DOMAIN SIZE

For sapphire, its thermal reffusivity is the inverse of  $\alpha$ , expressed as  $\Theta = 1/\alpha = 3/(v_l)$ .  $\Theta$  of our sample in comparison with those of two reference samples is plotted in Figure 3c. It is observed for both our sample and the literature sample that  $\Theta$  decreases monotonically with decreased  $T$  and reaches a constant at the 0 K limit. This can be explained by the fact that as temperature drops, the phonon-phonon scattering decreases and virtually vanishes near 0 K. Also, the  $\Theta$  of our sample is higher than that of the literature ones, reflecting the higher defect level in our sample.  $\Theta$  is affected by both defect and Umklapp scattering and is related to temperature as<sup>8</sup>

$$\Theta_i = \Theta_0 + C \times e^{-\theta_D/AT} \quad (5)$$

where  $C$  is a constant and  $\theta_D$  is the Debye temperature.  $\Theta_0$  is the residual thermal reffusivity at the 0 K limit:  $\Theta_0 = 3/(v_l)$ , where  $l_0$  is the phonon mean free path at the 0 K limit, also termed STD size. It is solely determined by defect-phonon scattering at the 0 K limit. The constant  $A$  is usually between 2 and 2.5 and takes 2 in our analysis. This constant is appropriate for cryogenic temperature situations that have been proved by various experiments.<sup>27</sup> It should be noted that the value of this constant will not affect the determination of  $\Theta_0$  and the STD size as  $\theta_D/A$  is fitted as a group. So, the value of  $A$  will only affect the estimation of  $\theta_D$ . Using eq 5, fitting is conducted on our results and the literature data. Once  $\Theta_0$  is obtained, STD size  $l_0$  can be determined as  $l_0 = 3/(v\Theta_0)^2$ .

For sapphire, at the 0 K limit, only the very low-energy acoustic phonons can be excited. From Figure 4a, we can conclude that these phonons also have a very low wave vector, meaning very low momentum. The acoustic phonon velocity at the 0 K limit can be calculated by studying the phonon dispersion relations of sapphire. Figure 4a shows the phonon dispersion relations in the in-plane direction of our sample,<sup>26</sup> the direction of  $k$ ,  $\alpha$ , and  $\Theta$  are measured. At the 0 K limit, three modes of acoustic phonons are analyzed to find the average phonon velocity: longitudinal acoustic (LA), flexural acoustic (ZA), and transverse acoustic (TA). When the frequency is low, the acoustic phonons have a linear dispersion. The velocity of each acoustic phonon branch is calculated to be 9990 m s<sup>-1</sup> for LA and 5480 m s<sup>-1</sup> for the ZA and TA modes. The average phonon velocity is calculated as

$$v = 3/(v_{LA}^{-1} + v_{TA}^{-1} + v_{ZA}^{-1}) \quad (6)$$

$v$  is found to be 6450 m s<sup>-1</sup>, which will be used for the STD size analysis.

Accurate determination of  $\Theta_0$  is critical for calculating the STD size. So, the relative standard deviation is used here in the fitting as it places the low-temperature data as equivalent important for fitting. It is defined as

$$\sigma = \sqrt{\sum (\Theta_i - f_i)^2 / \Theta_i^2 / N} \quad (7)$$

where  $f_i$  is the fitting data and  $N$  is the number of data points. The fitting results are shown in Figure 3c. The fitting results are summarized in Table 1. For the data from Roy,<sup>23</sup>  $\Theta_0$  is determined to be 0.135 sm<sup>-2</sup>, while for the data from Pishchik et al. [24], it is 0.179 sm<sup>-2</sup> (details of this small  $\Theta_0$  are shown in Figure 3d).

**Table 1. Summary of  $\Theta$ - $T$  Fitting Results for Our Sample and the Literature Samples**

sample	$\Theta_0$ (sm <sup>-2</sup> )	$C$ (sm <sup>-2</sup> )	$\theta_D$ (K)
ref 23	0.135	800,000	1329
ref 24	0.179	800,000	1310
$\mu\text{m}$ -thick sapphire wafer in this work	5460	800,000	966

The  $\Theta_0$  of our sample is 5460 sm<sup>-2</sup>, which is much higher than that of two literature studies by 4 orders of magnitude. This means that the crystallite size of our sample is much smaller than that of the two literature samples. Another point of contention is estimating  $\theta_D$  based on the variable  $A$  in eq 5. If  $A$  is 2,  $\theta_D$  determined for the literature data,<sup>23,24</sup> and our own results are 1329, 1310, and 966 K, respectively. These numbers are close to sapphire's Debye temperature reported in the literature: 1047 K.<sup>27</sup> For materials that rely on phonons for thermal transport, the Debye temperature can be easily extracted from the  $\Theta$  model, which can then be gauged as the strength of the atomic bonding in the sample. Based on  $\Theta_0$ , the STD size is calculated to be 2598  $\mu\text{m}$  for the sapphire in the literature<sup>24</sup> and 3445  $\mu\text{m}$  for the sapphire in the literature.<sup>23</sup> On the other hand, the STD size of our sample is determined to be 85.1 nm, much smaller than that of the two literature samples. This confirms that the  $\mu\text{m}$ -thick sapphire wafer studied in this work has more defects and grain boundaries, explaining its lower  $k$  shown in Figure 3b. For the samples reported in the literature,<sup>23</sup> they are single crystals with a much bigger size: 3–6 mm in thickness and length. This ensures a high crystalline structure much better than that of the 25  $\mu\text{m}$ -thick wafer used in this work. This explains the observed reduction in STD size and  $k$ .

As discussed in Section 2, the sapphire wafer has crystallite sizes of 283 nm in the cross-plane direction and 34.4 nm in the in-plane direction. In this work, the thermal conductivity is measured in the in-plane direction, so the STD size is more affected by the in-plane direction crystallite size. The STD size reflects the collective effects of both in-plane and cross-plane crystallite sizes. This explains why its value falls between them. If a crystalline material has the same crystallite sizes in all directions, it is expected the STD size will be close to the crystallite size. Therefore, the STD size can be treated as a structural characteristic size collectively affected by all direction crystallite sizes, with the crystallite size in the heat conduction direction having more effects. It should also be noted that if

the crystallite size is very large, for instance, in the order of mm, XRD is not able to characterize it since the induced XRD peak line width will be extremely small, even smaller than the machine limit. Under such a scenario, the STD size will provide very valuable information about the crystallite characteristic size.

## 6. CONCLUSIONS

In this work, with further development of the TET technique, the  $\alpha$  of a  $\mu\text{m}$ -thick sapphire wafer was measured at the limit of zero temperature rise. This is critical for uncovering the precise variation of  $\alpha$  with temperature, especially at cryogenic temperatures. The sapphire wafer was measured from 290 to 13 K, and its  $k$ ,  $\sigma$ , and  $\Theta$  were determined with high accuracy. The  $k$  of our studied  $\mu\text{m}$ -thick sapphire wafer is much lower than that of high-purity sapphire, which is attributed to the extensive grain boundaries in our sample. By fitting the  $\Theta$ - $T$  curve, the STD size of our sapphire wafer was determined to be 85.1 nm in the in-plane direction. This value is much smaller than that of high-purity sapphire crystals from the literature, namely, 2598 and 3445  $\mu\text{m}$ . The XRD analysis uncovered crystallite sizes of 283 nm in the cross-plane direction and 34.4 nm in the in-plane direction. The STD size reflects the collective effect of crystallite sizes in all directions, while that in the heat transfer direction plays a bigger role. For crystals of extremely high quality, their crystallite size could be too large to measure using XRD. For this situation, the STD size will become critical in uncovering the crystallite characteristic size, even in a lumped way.

## AUTHOR INFORMATION

### Corresponding Authors

**Huan Lin** – School of Environmental and Municipal Engineering, Qingdao University of Technology, Qingdao, Shandong 266033, P. R. China; [orcid.org/0000-0002-6475-0842](https://orcid.org/0000-0002-6475-0842); Email: [linhuan@qut.edu.cn](mailto:linhuan@qut.edu.cn)

**Xinwei Wang** – Department of Mechanical Engineering, 271 Applied Science Complex II, Iowa State University, Ames, Iowa 50011, United States; [orcid.org/0000-0002-9373-3750](https://orcid.org/0000-0002-9373-3750); Email: [xwang3@iastate.edu](mailto:xwang3@iastate.edu)

### Authors

**John Bai** – Department of Mechanical Engineering, 271 Applied Science Complex II, Iowa State University, Ames, Iowa 50011, United States

**Amin Karamati** – Department of Mechanical Engineering, 271 Applied Science Complex II, Iowa State University, Ames, Iowa 50011, United States

**Xinyue Duan** – College of New Energy, China University of Petroleum (East China), Qingdao, Shandong 266580, P. R. China

Complete contact information is available at: <https://pubs.acs.org/10.1021/acs.jpcc.5c00128>

### Notes

The authors declare no competing financial interest.

## ACKNOWLEDGMENTS

This work was partially supported by the US National Science Foundation (CMM12032464 for X.W.), the National Key Research and Development Program (2019YFE0119900 for

H.L.), and the Natural Science Foundation of Shandong Province (ZR2020ME183 for H.L.)

## REFERENCES

- (1) Xu, Z.; Wang, X.; Xie, H. Promoted electron transport and sustained phonon transport by DNA down to 10 K. *Polymer* **2014**, *55* (24), 6373–6380.
- (2) Xie, Y.; Xu, Z.; Xu, S.; Cheng, Z.; Hashemi, N.; Deng, C.; Wang, X. The defect level and ideal thermal conductivity of graphene uncovered by residual thermal reffusivity at the 0 K limit. *Nanoscale* **2015**, *7* (22), 10101–10110.
- (3) Zobeiri, H.; Hunter, N.; Xu, S.; Xie, Y.; Wang, X. Robust and high-sensitivity thermal probing at the nanoscale based on resonance Raman ratio (R3). *Int. J. Extreme Manuf.* **2022**, *4* (3), No. 035201.
- (4) Lian, Y.; Jiang, L.; Sun, J.; Zhou, J.; Zhou, Y. Ultrafast quasi-three-dimensional imaging. *Int. J. Extreme Manuf.* **2023**, *5* (4), No. 045601.
- (5) Xie, Y.; Wang, X. Thermal Conductivity of Carbon-based Nanomaterials: Deep Understanding of the Structural Effects. *Green Carbon* **2023**, *1*, 47–57.
- (6) Sivtsev, V.; Lapushkina, E.; Kovalev, I.; Guskov, R.; Popov, M.; Nemudry, A. Microtubular solid oxide fuel cells with a two-layer LSCF/BSCFM5 cathode. *Green Carbon* **2023**, *1* (2), 154–159.
- (7) Liu, J.; Xu, Z.; Cheng, Z.; Xu, S.; Wang, X. Thermal conductivity of ultrahigh molecular weight polyethylene crystal: defect effect uncovered by 0 K limit phonon diffusion. *ACS Appl. Mater. Interfaces* **2015**, *7* (49), 27279–27288.
- (8) Xie, Y.; Zhu, B.; Liu, J.; Xu, Z.; Wang, X. Thermal reffusivity: uncovering phonon behavior, structural defects, and domain size. *Front. Energy* **2018**, *12* (1), 143–157.
- (9) Lin, H.; Wang, R.; Zobeiri, H.; Wang, T.; Xu, S.; Wang, X. The in-plane structure domain size of nm-thick MoSe<sub>2</sub> uncovered by low-momentum phonon scattering. *Nanoscale* **2021**, *13* (16), 7723–7734.
- (10) Rahbar, M.; Li, B.; Hunter, N.; Al Keyyam, I.; Wang, T.; Shi, E.; Wang, X. Observing grain boundary-induced phonons mean free path in highly aligned SWCNT bundles by low-momentum phonon scattering. *Cell Rep. Phys. Sci.* **2023**, *4* (12), No. 101688.
- (11) Han, M.; Liu, J.; Xie, Y.; Wang, X. Sub- $\mu\text{m}$  c-axis structural domain size of graphene paper uncovered by low-momentum phonon scattering. *Carbon* **2018**, *126*, 532–543.
- (12) Mohammed, A. A.; Khodair, Z. T.; Khadam, A. A. Preparation and investigation of the structural properties of  $\alpha$ -Al<sub>2</sub>O<sub>3</sub> nanoparticles using the sol-gel method. *Chem. Data Collect.* **2020**, *29*, No. 100531.
- (13) Zilberberg, L.; Mitlin, S.; Shankar, H.; Asscher, M. Buffer Layer Assisted Growth of Ag Nanoparticles in Titania Thin Films. *J. Phys. Chem. C* **2015**, *119*, 28979–28991.
- (14) Graf, D.; Molitor, F.; Ensslin, K.; Stampfer, C.; Jungen, A.; Hierold, C.; Wirtz, L. Spatially resolved Raman spectroscopy of single- and few-layer graphene. *Nano Lett.* **2007**, *7* (2), 238–242.
- (15) Lee, W.-J.; Chang, Y.-H. Growth without Postannealing of Monoclinic VO<sub>2</sub> Thin Film by Atomic Layer Deposition Using VCl<sub>4</sub> as Precursor. *Coatings* **2018**, *8*, No. 431.
- (16) Xu, S.; Tang, X.; Yue, Y.; Wang, X. Sub-micron imaging of sub-surface nanocrystalline structure in silicon. *J. Raman Spectrosc.* **2013**, *44* (11), 1523–1528.
- (17) Zhu, B.; Wang, R.; Harrison, S.; Williams, K.; Goduguchinta, R.; Schneiter, J.; Pegna, J.; Vaaler, E.; Wang, X. Thermal conductivity of SiC microwires: Effect of temperature and structural domain size uncovered by 0 K limit phonon scattering. *Ceram. Int.* **2018**, *44* (10), 11218–11224.
- (18) Lin, H.; Xu, S.; Wang, X.; Mei, N. Thermal and Electrical Conduction in Ultrathin Metallic Films: 7 nm down to Sub-Nanometer Thickness. *Small* **2013**, *9* (15), 2585–2594.
- (19) Liu, J.; Wang, T.; Xu, S.; Yuan, P.; Xu, X.; Wang, X. Thermal conductivity of giant mono- to few-layered CVD graphene supported on an organic substrate. *Nanoscale* **2016**, *8* (19), 10298–10309.
- (20) Zhu, B.; Liu, J.; Wang, T.; Han, M.; Valloppilly, S.; Xu, S.; Wang, X. Novel Polyethylene Fibers of Very High Thermal

Conductivity Enabled by Amorphous Restructuring. *ACS Omega* **2017**, *2* (7), 3931–3944.

(21) Hunter, N.; Karamati, A.; Xie, Y.; Lin, H.; Wang, X. Laser Photoreduction of Graphene Aerogel Microfibers: Dynamic Electrical and Thermal Behaviors. *ChemPhysChem* **2022**, *23* (23), No. e202200417.

(22) Guo, J. Q.; Wang, X. W.; Wang, T. Thermal characterization of microscale conductive and nonconductive wires using transient electrothermal technique. *J. Appl. Phys.* **2007**, *101* (6), No. 063537.

(23) Roy, F. Modeling and Characterization of Coated Conductors Applied to the Design of Superconducting Fault Current Limiters. Ph.D. Thesis; EPFL, 2010.

(24) Dobrovinskaya, E. R.; Lytvynov, L. A.; Pishchik, V. Properties of Sapphire. In *Sapphire: Material, Manufacturing, Applications*; Springer, 2009; pp 55–176.

(25) Siemens, M. E.; Li, Q.; Yang, R.; Nelson, K. A.; Anderson, E. H.; Murnane, M. M.; Kapteyn, H. C. Quasi-ballistic thermal transport from nanoscale interfaces observed using ultrafast coherent soft X-ray beams. *Nat. Mater.* **2010**, *9* (1), 26–30.

(26) Schober, H.; Strauch, D.; Dorner, B. Lattice dynamics of sapphire ( $\text{Al}_2\text{O}_3$ ). *Z. Phys. B: Condens. Matter* **1993**, *92* (3), 273–283.

(27) Kittel, C.; McEuen, P. *Introduction to Solid State Physics*; John Wiley & Sons, 2018.